

Reflectivity and photoluminescence measurements in ZnS epilayers grown by metal-organic chemical-vapor deposition

A. Abounadi, M. Di Blasio, D. Bouchara, J. Calas, M. Averous, O. Briot, N. Briot, T. Cloitre, R. L. Aulombard, and B. Gil

Groupe d'Etudes des Semiconducteurs, URA 357, Université Montpellier II, 34095 Montpellier Cedex 05, France

(Received 23 February 1994; revised manuscript received 13 June 1994)

Thin films of high-quality ZnS were grown on (001) GaAs and (111) Si substrates by metal-organic chemical-vapor deposition. 2-K reflectivity was used to analyze various samples grown at different temperatures. The spectra show two structures at 3.801 eV corresponding to the free exciton and at 3.871 eV corresponding to the $E_0 + \Delta_0$ transition. Theoretical reflectivity spectra were calculated using the spatial dispersion model with two oscillators. Thus, the transverse energies, the longitudinal transversal splitting, the oscillator strengths, and the damping parameters were determined for both the free exciton and the split-off exciton of ZnS. Photoluminescence measurements were also carried out using an excimer laser (308 nm). Both light-hole and heavy-hole excitons were observed, which allow for the determination of the strain that exists in the layer. This strain is due only to the difference between the thermal-expansion coefficients of the GaAs substrate and the ZnS epilayer, and was demonstrated to be a tensile strain. This paper also presents results on the band-gap energy variation as a function of the temperature and photoluminescence spectra when the excitation was varied from weak to very high densities (15 MW/cm²).

I. INTRODUCTION

Recent interest in the epitaxial growth of II-VI wide-gap materials originates from their potential application for short-wavelength, namely, the green to ultraviolet, light-emitting devices. Such devices could be light-emitting diodes (LED's) or laser diodes.^{1,2} The materials that are presently being studied for such uses are ZnSe, ZnTe, ZnS, and their superlattices and alloys. Among these materials studies have been extensively carried out on ZnSe and ZnTe. To a lesser extent, studies are now starting on ZnS. ZnS is the primary candidate for ultraviolet emitting devices as a consequence of its large energy band gap of 3.7 eV at room temperature. Recently, high-quality thin-film layers of ZnS have been grown by metal-organic chemical-vapor deposition (MOCVD) and molecular-beam epitaxy (MBE).³⁻⁶ Both techniques allow for lower growth temperatures when compared to other growth techniques, essentially achieving higher-quality layers. The results concerning the growth conditions and the characterization by double x-ray diffraction are published elsewhere.⁵ The purpose of this paper is to present results obtained in reflectivity and photoluminescence experiments and a theoretical reflectivity calculation.

The theoretical reflectivity model is based on a spatial dispersion method with two oscillators. Also included in this work is a study on the temperature dependence of the energy band gap, the dependence on the growth temperature, and the calculation of the thermal strain, since the layer suffers two-dimensional tensile stress.

II. EXPERIMENTAL AND THEORETICAL REFLECTIVITY RESULTS

A. Experimental results

The reflectivity experiments were performed with a deuterium lamp as the excitation source in a standard setup. The deuterium lamp was an ideal source since it emits a stable linear spectrum in the wavelength region of 3150–3350 Å. The experiments were performed on four samples fabricated under different growth conditions. Table I contains these specifications.

The reflectivity curves obtained at 2 K are illustrated in Fig. 1. Two well-defined structures are observable for the samples grown on the GaAs substrate, while the sample grown on Si is of lower quality. The latter's poor quality is due to the antiphase defects caused by the non-

TABLE I. ZnS sample specifications with a VI/II molar ratio of 5 for all the samples.

Sample number	Layer/substrate	Growth temperature (°C)	Layer thickness (μm)
1	ZnS/GaAs	300	0.8
2	ZnS/GaAs	350	1.0
3	ZnS/GaAs	400	0.8
4	ZnS/Si	300	1.0

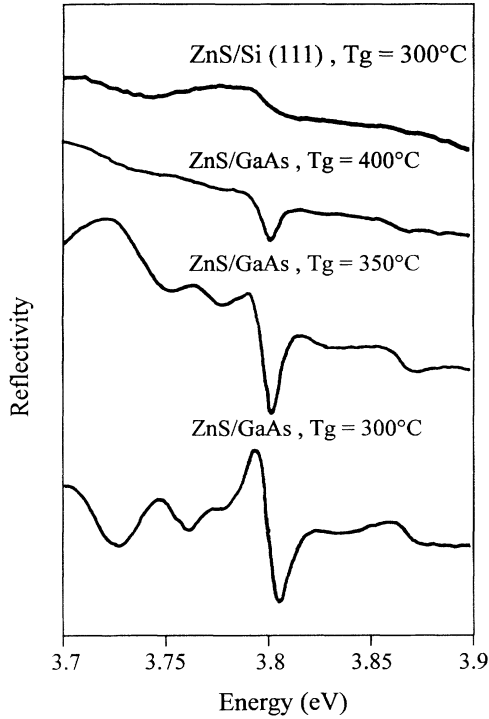


FIG. 1. Substrate and growth-temperature (T_g) dependence of reflectivity spectra taken at 2 K of various ZnS layers. The free-exciton and the spin-orbit splitting structures are visible at 3.801 and 3.871 eV, respectively.

polarity of the substrate.⁷ In the former cases, the two structures that appear at 3.801 and 3.871 eV, respectively, correspond to the transition of the free exciton and the Γ_6 - Γ_7 transition. The Γ_6 - Γ_7 transition is used experimentally to determine the splitting Δ_0 caused by the spin-orbit interaction. Δ_0 was found to be on the order of 70 meV, which confirms the results of Bir *et al.*,⁸ and those reported by Eckelt⁹ and Shahzad and Olego.¹⁰ The mismatch between the lattice constants of ZnS and GaAs is 4.5%, generating a critical thickness of a few monolayers (10–40 Å) for the thin film.¹¹ The thickness of the samples on which the experiments were performed is of the order of 1 μm . These layers are entirely relaxed and only the strain due to the difference between the thermal-expansion coefficients exists ($6.7 \times 10^{-6} \text{ K}^{-1}$ for ZnS and $5.7 \times 10^{-6} \text{ K}^{-1}$ for GaAs at 300 K). The heavy-hole–light-hole splitting is not observable. This we attribute to the large area of the epilayer under the spot of the deuterium lamp and the subsequent sampling of ZnS regions that display different strain states. This gives broader structures than when using more localized excitation like a laser beam. In the photoluminescence spectra, taken using a more strongly focused excitation radiation than in reflectance, this splitting was observed, consequently allowing the strain to be determined.

B. Reflectivity versus temperature

The free-exciton and the spin-orbit transition peaks are uniformly shifted toward lower energies when the tem-

perature is increased. The results for sample 1 are illustrated in Fig. 2. The temperature variation is defined by two different curvature characteristics. The first describes a nonlinear law for temperatures less than 80 K; this law is an extension of Varshni's relation and is represented by

$$E(T) = E(0) - \frac{\alpha T^4}{\beta + T^3}$$

with

$$\alpha = 4.01 \times 10^{-4} \text{ eV/K},$$

$$\beta = 2 \times 10^6 \text{ K}^3.$$

The second law for temperatures greater than 80 K is described by the linear variation

$$E(T) = E(0) + \gamma + \xi T$$

with

$$\xi = -4.7 \times 10^{-4} \text{ eV/K},$$

$$\gamma = 25.4 \text{ meV}.$$

C. Reflectivity study using a spatial dispersion model with two oscillators

The dielectric behavior can be written as a sum over the resonances, each resonance occurring at a particular frequency. The spatial dispersion (i.e., nonlocal dielectric behavior) effect that is considered presently is the wave-vector dependence of the resonant frequencies on the op-

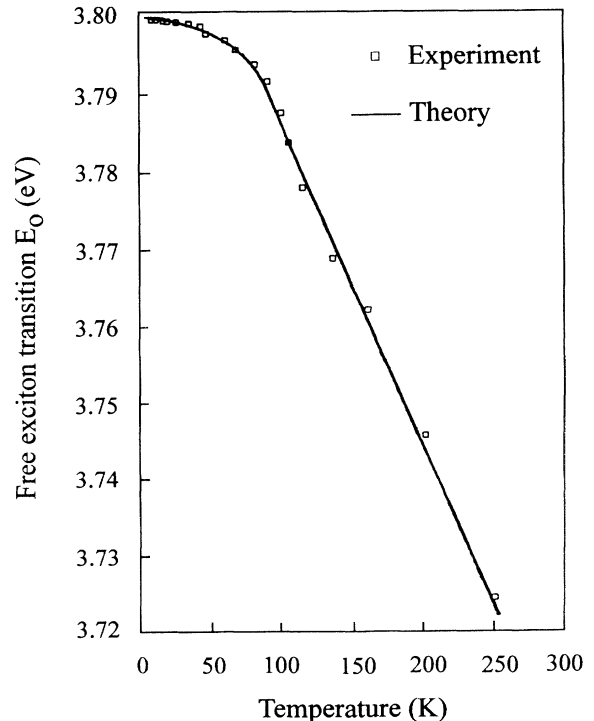


FIG. 2. Free-exciton transition evolution versus temperature. Both experimental and theoretical data are represented.

tical properties. Thus, there exist three propagating modes inside the crystal. For such a theory the reflectivity calculation requires additional boundary conditions to describe the electromagnetic field inside the crystal. These boundary conditions and the notion of the dead layer are generalized from the one-oscillator model of Hopfield and Thomas.¹²

Theory

In general, insulating crystals are characterized by polarizabilities of the form

$$\alpha(\mathbf{k}, \omega) = \sum_j \frac{\alpha_j(\mathbf{k})\omega_j^2(\mathbf{k})}{\omega_j^2(\mathbf{k}) - \omega^2 - i\omega\Gamma_j(\mathbf{k})},$$

where j represents the summation index on the different optical absorption lines. Only the effect of finite exciton mass is investigated. The reflectivity spectra are characterized by the two peaks related to the free exciton around 3.801 eV and the spin-orbit splitting around 3.871 eV (Table II gives the exactly determined energy position from the following model). Thus the summation has to be carried out over the contribution of the two oscillators, while the sum over all the other oscillators is grouped into the background dielectric constant ϵ_b . The general solution, periodic in space and time, to Maxwell's equations is found by solving

$$k^2 \mathbf{E}_k - \mathbf{k}(\mathbf{E}_k \cdot \mathbf{k}) = \frac{\omega^2}{c^2} \mathbf{D}_k = \frac{\omega^2}{c^2} (\mathbf{E}_k + 4\pi \mathbf{P}_k). \quad (1)$$

The solution of Eq. (1) is divided into longitudinal and transverse solutions. Using the approximation stated above, and for particular experimental conditions, only one solution will be taken into account. For normal incidence and a single transverse polarization, all the wave vectors involved in the problem are collinear, and the longitudinal modes are not excited. The dielectric constant is then given by

$$\epsilon(\mathbf{k}, \omega) = \epsilon_b + \sum_{j=1}^2 \frac{4\pi\alpha_{0j}\omega_{0j}^2}{\omega_{0j}^2 + (\hbar k^2/m_j^*)\omega_{0j} - \omega^2 - i\omega\Gamma},$$

where ϵ_b is the background dielectric constant, ω_{0j} is the transverse frequency relate to the exciton j with an effective mass of m_j^* , $A_j = 4\pi\alpha_{0j}$ is the polarizability of the excitonic resonances at $\omega=0$ and $k=0$ (oscillator

strength), and Γ_j is the damping parameter corresponding to the excitonic transitions, which depends on the interactions with the phonons and intrinsic and extrinsic defects. Since $k = \omega n/c = \sqrt{\epsilon_r}\omega/c$ where $\epsilon_r = \epsilon(\mathbf{k}, \omega) = k^2 c^2/\omega^2$, by making the transformations

$$X_j = A_j \omega_j^2 \left[\frac{m_j^* c^2}{\hbar \omega_j \omega^2} \right]$$

and

$$Y_j = (\omega_j^2 - \omega^2 - i\omega\Gamma_j) \left[\frac{m_j^* c^2}{\hbar \omega_j \omega^2} \right]$$

for $j=1,2$, we obtain $\epsilon(k, \omega)$ as the solution of the third-order equation

$$\epsilon^3 + \epsilon^2 [Y_1 + Y_2 \epsilon_b] + \epsilon [Y_1 Y_2 - X_1 - X_2 - \epsilon_b (Y_1 + Y_2)] - [\epsilon_b Y_1 Y_2 + X_1 Y_2 + X_2 Y_1] = 0. \quad (2)$$

There are three transverse exciton polarization modes inside the crystal, $k_i^2 = \epsilon_i \omega^2/c^2$, where ϵ_i for $i=1,2,3$ are the solution of Eq. (2). From the polariton branches the longitudinal frequencies can also be determined:

$$\omega_{Lj} = \omega_{0j} \left[1 + \frac{4\pi\alpha_{0j}}{\epsilon_b} \right]^{1/2}.$$

The longitudinal transversal splitting can then be approximated by

$$E_{LTj} = E_{Lj} - E_{0j} \approx \frac{2\pi\alpha_{0j}}{\epsilon_b} E_{0j} = \frac{A_j}{2\epsilon_b} E_{Tj}.$$

The Maxwell boundary conditions, i.e., the conservation of the tangential components of \mathbf{E} and \mathbf{B} , at the surface must be satisfied:

$$E_0 + E_R = E_1 + E_2 + E_3,$$

$$(E_0 - E_R) = n_1 E_1 + n_2 E_2 + n_3 E_3,$$

where $n_i = ck_i/\omega$ ($i=1,2,3$), k_i is the right running root of the dispersion relation given by $c^2 k^2/\omega^2 = \epsilon(\mathbf{k}, \omega)$. From the last two equations, one sees that two other equations are needed to determine the solution for the reflection coefficient $|E_R/E_0|^2$. For this, the Pekar condition is applied. This condition states that the exciton

TABLE II. Results of the fitting parameters for various ZnS layers grown on different substrates.

Substrate	GaAs(001)			Si(111)
Growth temperature (°C)	300	350	400	400
E_0 transition (eV)	3.8005	3.7995	3.799	3.799
$E_0 + \Delta_0$ transition (eV)	3.870	3.870	3.869	3.870
$4\pi\alpha_0(E_0)$	6.4×10^{-3}	5×10^{-3}	4.3×10^{-3}	2.9×10^{-3}
$4\pi\alpha_0(E_0 + \Delta_0)$	2.4×10^{-3}	1.9×10^{-3}	1.6×10^{-3}	1.5×10^{-3}
$E_{LT}(E_0)$ (meV)	2.1	1.64	1.41	NA
$E_{LT}(E_0 + \Delta_0)$ (meV)	0.8	0.63	0.53	NA
$\Gamma(E_0)$ (meV)	6.3	10	12.5	28
$\Gamma(E_0 + \Delta_0)$ (meV)	15	19.7	22	38
Dead-layer thickness (Å)	15	30	42	600

moving from the right to the left side of the crystal is totally reflected by a potential that takes into account the interaction between the exciton and its image charge, as well as the surface effects. As a consequence, there exists a layer called the "dead layer" that the exciton cannot exist within. Its thickness is not well defined,¹² but estimated to be of the order of the exciton effective Bohr radius.^{13,14} The problem is then reduced to one of three layers, where the limit conditions are those of Maxwell appended by the Pekar condition. Therefore the exciton does not exist beyond a certain distance within the crystal and its contribution to the polarization past this limit is zero. $P_{\text{ex}}=0$ for $x=L$, where L is the thickness of the

dead layer. We then have the following formulas:

$$n_b(E'_0 + E'_R) = E_1 + E_2 + E_3,$$

$$n_b(E'_0 - E'_R) = n_1 E_1 + n_2 E_2 + n_3 E_3,$$

$$P_{\text{ex,1tot}} = 0 \iff \sum_{i=1}^3 P_{1,i} = \sum_{i=1}^3 \frac{X_1}{Y_1 + \epsilon_i} E_i = 0,$$

$$P_{\text{ex,2tot}} = 0 \iff \sum_{i=1}^3 P_{2,i} = \sum_{i=1}^3 \frac{X_2}{Y_2 + \epsilon_i} E_i = 0.$$

The analytic expression of the reflection coefficient is given by

$$\left| \frac{E_R}{E_0} \right|^2 = \left| \frac{a_1(b_2 F_3 - b_3 F_2) - a_2(b_1 F_3 - b_3 F_1) - a_3(b_2 F_1 - b_1 F_2)}{a_1(b_2 H_3 - b_3 H_2) - a_2(b_1 H_3 - b_3 H_1) - a_3(b_3 H_1 - b_1 H_2)} \right|^2,$$

where $a_i = 1/(Y_1 + \epsilon_i)$ and $b_i = 1/(Y_2 + \epsilon_i)$, and

$$F_i = n_i Z_1 + n_b Z_2, \quad H_i = n_i Z_3 + n_b Z_4,$$

$$Z_1 = n_b(u+1) - (u-1), \quad Z_3 = n_b(u+1) + (u-1),$$

$$Z_2 = n_b(u-1) - (u+1), \quad Z_4 = n_b(u-1) + (u+1),$$

for $i=1, 2$, and 3 , $u = e^{-2ik_b L}$, $k_b = \sqrt{\epsilon_b} \omega/c$, and $n_b = \sqrt{\epsilon_b}$.

The adjustable parameters are ϵ_b , A_1 , A_2 , ω_1 , ω_2 , Γ_1 , Γ_2 , and L . The effective masses are taken from Ref. 15. $m_e^* = 0.28m_0$, $m_h^* = 0.61m_0$. The effective translational exciton masses are then equal to $m_1^* = 0.89m_0$ for the free exciton and $m_2^* = 1.12m_0$ for the split-off exciton. The last one was taken as an adjustable parameter since we could not find values of effective mass for the lower valence band Γ_7 . It should be mentioned that there is a large variation even for m_e^* and m_h^* in the literature but the theoretical curves are not very sensitive to a slight

variation of the translational exciton masses. Using the effective-mass approximation for the bulk modulus, for which the binding energy R^* corresponding to the fundamental state of the free exciton is equal to 40 meV, the effective Bohr radius is calculated as $a_0^* = a_0 \epsilon m_0 / \epsilon_0 \mu$ where a_0 is the Bohr radius, $\epsilon = 8.32\epsilon_0$ is the static dielectric constant,¹⁶ and μ is the reduced free-exciton effective mass. a_0^* is about 22 Å. Figures 3 and 4 illustrate the experimental and theoretical reflectivity curves and the results of the fit are listed in Table II.

For the layer grown on Si(111) we were not able to fit the experimental reflectivity well using the spatial dispersion model. The values reported in Table II are calculated from a local description model. One can notice the following.

- (i) The dead-layer thickness for the sample grown at 300 °C is less than but close to the Bohr radius.
- (ii) We obtained $\epsilon_b = 5.8\epsilon_0$ in good agreement with the dynamic dielectric constant ($\epsilon_\infty = 5.7\epsilon_0$).¹⁷
- (iii) The broadening parameters we fitted in our sam-

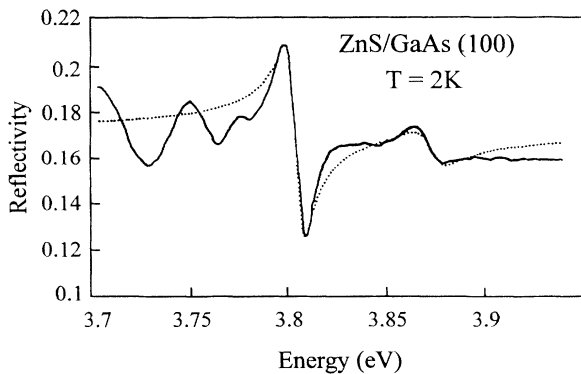


FIG. 3. Experimental 2-K reflectivity spectrum (solid line) and calculated spectrum (dashed line) of a 1- μm -thick ZnS layer grown on (001) GaAs substrate.

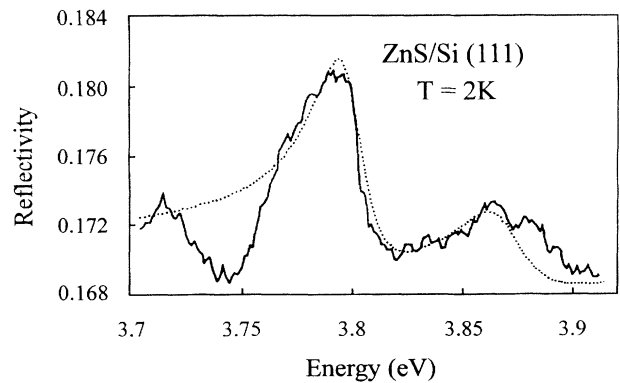


FIG. 4. Experimental 2-K reflectivity spectrum (solid line) and calculated spectrum (dashed line) of a 1- μm -thick ZnS layer grown on (111)Si substrate.

ples are relatively important. This is attributed to the high density of interfacial dislocation, due to the layer relaxation, which results from the large mismatch between the lattice constants of ZnS and GaAs (4.5%).

(iv) The oscillator-strength ratio is almost constant for the layers grown on GaAs.

III. PHOTOLUMINESCENCE RESULTS AND DISCUSSION

A. Experimental results

At 4.2 K, the energy gap of ZnS is equivalent to 3.84 eV. It is very difficult to observe the band edge using a He-Cd laser ($\lambda_{\text{exc}} = 3250 \text{ \AA}$). Therefore a Xe-Cl excimer laser with an excitation wavelength of 308 nm is used. To avoid high-density effects, a neutral-density filter is used (intensities $\leq 1 \text{ kW/cm}^2$). Figure 5 illustrates the photoluminescence results. Two structures are visible: the first one at 326.46 nm corresponds to the light-hole exciton¹⁸ and the second one at 326.2 nm to the heavy-hole exciton. These peaks are the result of the energy transitions caused by the thermoelastic strain due to the difference between the thermal energy transitions caused by the thermoelastic strain due to the difference between the thermal expansion coefficients of ZnS and GaAs. Another structure at 326.98 nm (I_2) is also observed. It is attributed to an exciton bound to a neutral donor. Kawakami Taguchi, and Hiraki,¹⁹ using intentional doping with I and Na, observed a small increase of this peak when iodine doping increases. Thus this peak is due not only to the native defects but also to the contamination by impurities. At 331.18 nm another peak is visible and is attributed by the same authors to an exciton bound to a neutral acceptor (Na), I_1 . The appearance of these impurities in the fabrication process cannot be explained even though these peaks appeared at the same energy values as those identified as impurities in Ref. 19.

Maintaining the excitation density constant, the intensity ratio of the free-exciton structure (I_{hh} for samples grown at 300°C and 350°C, E_x for the one grown at

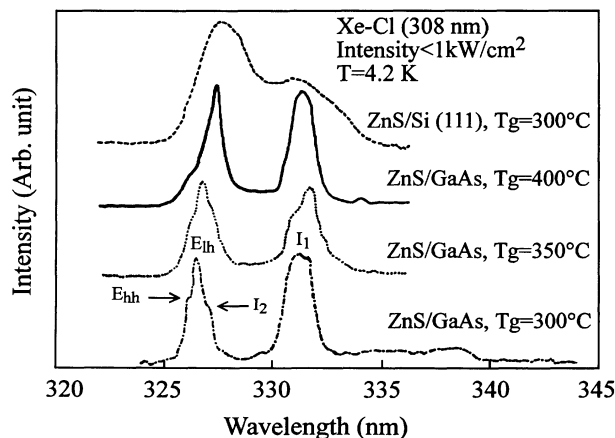


FIG. 5. Substrate and temperature dependence of 4.2-K photoluminescence spectra.

400°C) to the bound-exciton line (I_2 for the donor and I_1 for the acceptor) was compared. For the sample fabricated at 400°C, the heavy-hole–light-hole splitting was not observed, but a relatively weak structure E_x , when compared to the bound-exciton peaks, appeared at 326.29 nm. Keeping in mind the damping parameters and the oscillator forces determined from the model used to fit the reflectivity experimental results, one deduces that the layer grown at 300°C is of a higher quality than those grown at 350°C and 400°C. Thus a low growth temperature is highly desirable since it reduces the defect density.

B. Effect of strain on the electronic band structure of ZnS/GaAs epilayers grown along the (001) axis

For a zinc-blende-type material, the valence bands at the center of the Brillouin zone consist of a fourfold $P_{3/2}$ manifold ($J = \frac{3}{2}$, $m_j = \pm \frac{3}{2}, \pm \frac{1}{2}$) and a $P_{1/2}$ doublet ($J = \frac{1}{2}$, $m_j = \pm \frac{1}{2}$). The biaxial strain reduces the symmetry from T_d and thus splits the $P_{3/2}$ manifold into an $m_j = \pm \frac{1}{2}$ (light-hole) and an $m_j = \pm \frac{3}{2}$ (heavy-hole) subband. Also the hydrostatic stress component of the strain shifts the gravity center of the $P_{3/2}$ manifold and the $P_{1/2}$ doublet with respect to the conduction band. The transitions between these valence bands and the lowest conduction band at $k=0$ are labeled E_{lh} , E_{hh} , and $E_0 + \Delta_0$, respectively, where Δ_0 is the spin-orbit splitting of the valence band at $k=0$. The energy change of the $J = \frac{3}{2}$ and $J = \frac{1}{2}$ states relative to the conduction-band minimum induced by the strain can be calculated by the Hamiltonian matrix which uses the unperturbed wave functions. The energy shifts with respect to its zero-stress value for excitonic transitions associated with Γ_6 , Γ_8 and Γ_6 - Γ_7 band extrema are thus given by

$$\begin{aligned} \Delta E_{\text{lh}} &= \left[2a \left(\frac{c_{11} - c_{12}}{c_{11}} \right) + b \left(\frac{c_{11} + 2c_{12}}{c_{11}} \right) \right] \epsilon, \\ \Delta E_{\text{hh}} &= \left[2a \left(\frac{c_{11} - c_{12}}{c_{11}} \right) - b \left(\frac{c_{11} + 2c_{12}}{c_{11}} \right) \right] \epsilon, \\ \Delta(E_0 + \Delta_0) &= 2a \left(\frac{c_{11} - c_{12}}{c_{11}} \right) \epsilon. \end{aligned} \quad (3)$$

Here c_{ij} are the elastic stiffness constants of ZnS, a is the hydrostatic deformation potential characterizing the relative energy shift of Γ_6 from the valence band (Γ_8 and Γ_7) under the hydrostatic component, b is the valence band's shear deformation potential, and $\epsilon = \Delta a / a_{\text{ZnS}}$ is the in-plane residual strain in the layer (with $\Delta a = a_{\text{ZnS}} - a_{\parallel}$, where a_{\parallel} is the in-plane lattice parameter). In this particular case, the residual strain is caused by the thermal strain induced by the difference of the thermal-expansion coefficients. From the shift of the excitonic emission features (almost 1 meV for E_{lh} which moves strongly when ϵ varies) to lower energies when the growth temperature increases from 300 to 350°C (the thermoelastic strain which varies as $\Delta T = T_g - T_{\text{exp}}$ is then increased), we conclude that the stress is a tensile thermoelastic one.

Unfortunately, the quality of the sample grown at 400 °C is worse, and the near-band-edge photoluminescence displays less information than for samples grown at lower temperature. This overall behavior agrees with the study of the interface stress of MOCVD-grown $\text{ZnS}_x\text{Se}_{1-x}/\text{GaAs}$ of Tonami *et al.*²⁰ where they demonstrated that a tensile strain exists within layers of thickness greater than the critical value, regardless of the composition x . Different combinations of Eqs. (3) allow us to estimate the value of the strain:

$$E_{\text{lh}} - E_{\text{hh}} = \Delta E_{\text{lh}} - \Delta E_{\text{hh}} = 2b \left[\frac{c_{11} + 2c_{12}}{c_{11}} \right] \varepsilon$$

$$\Rightarrow \varepsilon = \frac{E_{\text{lh}} - E_{\text{hh}}}{2b[(c_{11} + 2c_{12})/c_{11}]}$$

Using the subsequent values $E_{\text{lh}} = 3.797$ eV, $E_{\text{hh}} = 3.800$ eV, $a = -4.53$ eV,²¹ $b = -1.25$ eV,¹⁰ $c_{11} = 10.40 \times 10^{10}$ N/m²,²² and $c_{12} = 6.50 \times 10^{10}$ N/m²,²² the calculated residual strain ε is then estimated to be -0.53×10^{-3} for the sample grown at 300 °C and -0.62×10^{-3} for the sample grown at 350 °C. This determination of the magnitude and sign of the residual strain has been completed by a calculation in the spirit of the ideas developed by Shibata *et al.*²³ and Gutowski, Presser, and Kudlek²⁴ for the study of the residual strain in ZnSe epilayers grown onto GaAs. Following these authors, the accurate determination of the deformation can be obtained analytically as a combined function of the differences between growth temperature and temperature of the experiment, and of the thermal-expansion coefficients and lattice parameters of both the substrate and epilayer compound [see, for instance, Eq. (2.6) of Ref. 24]. Making such a calculation we obtain $\varepsilon = -0.57 \times 10^{-3}$ -0.6×10^{-3} at 300 and

350 °C, respectively. Both the sign and magnitude of ε so determined are in agreement with the value calculated from the experiment. This is a strong additional support to the attribution of the 3.797 eV line to the light-hole exciton not seen in reflectivity.

C. High-excitation-density experiment

To complete this study of optical properties of the ZnS epilayer we have varied the pump power density. Figure 6 illustrates the evolution of the photoluminescence spectra when increasing the excitation density over four decades. At low excitation densities we detect both near-band-edge (heavy-hole, light-hole, and I_2) excitons and deeper ones (I_1). For excitations greater than several hundred kW/cm², a broadband emission appears and dominates the spectrum. This emission may be related to electron-hole-drop creation.^{25,26} The half-width of this band increases and its position shifts toward longer wavelengths as excitation intensities increase, due to the onset of many-body effects and band-gap renormalization.

IV. CONCLUSION

High-quality MOCVD ZnS layers were grown on different substrates and at different temperatures. Reflectivity and photoluminescence experiments and theoretical reflectivity calculations based on the spatial dispersion model with two oscillators were studied. The spin-orbit splitting Δ_0 (70 meV) was experimentally determined from the reflectivity spectra. The reflectivity versus temperature was studied. Two different curvatures describe the energy variation: a nonlinear law for temperatures less than 80 K and a linear one for those above this temperature. Light-heavy hole splitting was observed in the photoluminescence spectra (using a Xe-Cl laser, 308 nm). Thus the residual tensile strain, due only to the difference between the thermal-expansion coefficients of the layer and the substrate, was calculated. Its value is equal to -0.53×10^{-3} . Comparing the layers' optical spectra, one can see that ZnS grown on Si(111) is of a poorer quality. This was explained in terms of antiphase defects resulting from the nonpolarity of the substrate. For the layers grown on GaAs(001) at different temperatures the reflectivity model used permitted us to determine the fitting parameters (oscillator strengths, damping parameters, and the dead-layer thickness). Using these parameters and comparing the intensity ratios of the samples, the layer grown at 300 °C was demonstrated to be of higher quality. This is important as a low growth temperature is needed to reduce the native defect density.

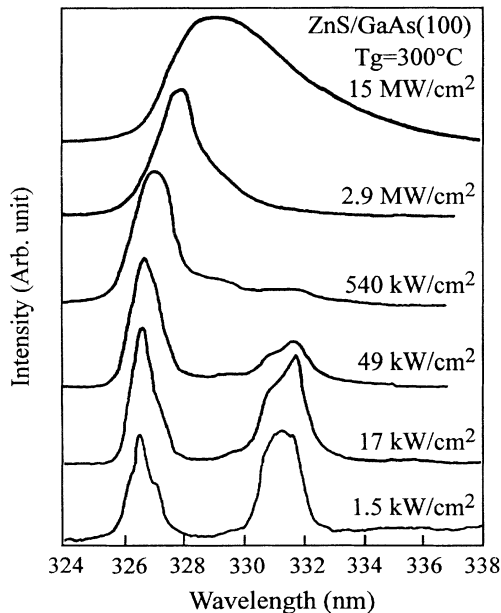


FIG. 6. 4.2-K photoluminescence spectra of the ZnS layer at various excitation densities. The maximum excitation density is 15 MW/cm² and the minimum is 1.5 kW/cm².

ACKNOWLEDGMENTS

The authors would like to thank A. Chergui, B. Hönerlage, R. Levy, and J. Valenta, from Groupe d'Optique Non-Linéaire et d'Optoélectronique, Institut de Physique de Strasbourg, for photoluminescence experiments.

- ¹R. Gunshor, A. Nurmikko, and M. Koyabashi, *Phys. World* **5**, 460 (1992).
- ²J. Qui, J. M. DePuydt, H. Cheng, and M. A. Haase, *Appl. Phys. Lett.* **59**, 2992 (1991).
- ³Y. Kawakami, T. Taguchi, and A. Hiraki, *J. Vac. Sci. Technol. B* **5**, 1171 (1987).
- ⁴T. Yodo, K. Ueda, K. Moriro, K. Yamashita, and S. Tanaka, *J. Appl. Phys.* **63**, 5674 (1990).
- ⁵O. Briot, N. Briot, A. Aboundai, B. Gil, T. Cloitre, and R. L. Aulombard, *Semicond. Sci. Technol. Lett.* **9**, 207 (1994).
- ⁶M. Yontea, M. Ohishi, H. Saito, and T. Hamasaki, *J. Cryst. Growth* **127**, 314 (1993).
- ⁷D. B. Holt, *J. Phys. Chem. Solids* **30**, 1297 (1969).
- ⁸G. L. Bir, G. E. Pikus, L. G. Sustinata, and A. L. Fedorova, *Fiz. Tverd. Tela (Leningrad)* **12**, 1187 (1970) [*Sov. Phys. Solid State* **12**, 926 (1970)].
- ⁹P. Eckelt, *Solid State Commun.* **6**, 489 (1968).
- ¹⁰K. Shahzad and D. J. Olego, *Phys. Rev. B* **38**, 1417 (1988).
- ¹¹M. Henken, *Mater. Sci. Eng. B* **9**, 189 (1991).
- ¹²J. J. Hopfield and D. G. Thomas, *Phys. Rev.* **132**, 563 (1963).
- ¹³A. D'Andrea and R. Del Sole, *Phys. Rev. B* **25**, 3714 (1982).
- ¹⁴S. Satpathy, *Phys. Rev. B* **28**, 4585 (1983).
- ¹⁵P. E. Lippens and M. Lannoo, *Phys. Rev. B* **39**, 10 935 (1989).
- ¹⁶G. Martins, R. Girlanda, N. Tomassini, A. D'Andrea, and R. Atanasov, *J. Phys. (Paris) Colloq.* **54**, C5-413 (1993).
- ¹⁷A. Manabe, A. Mitsubishi, and H. Yoshinaga, *Jpn. J. Appl. Phys.* **6**, 593 (1967).
- ¹⁸T. Ohno and T. Taguchi, *J. Cryst. Growth* **107**, 649 (1991).
- ¹⁹Y. Kawakami, T. Taguchi, and A. Hiraki, *J. Cryst. Growth* **89**, 331 (1988).
- ²⁰Y. Tonami, J. Nishimo, Y. Hamakawa, T. Sakamoto, and S. Fujita, *Jpn. J. Appl. Phys.* **27**, L6506 (1988).
- ²¹S. Ves, U. Schwartz, N. E. Christensen, K. Syassen, and M. Cardona, *Phys. Rev. B* **42**, 9113 (1990).
- ²²R. K. Singh and Sadhna Singh, *Phys. Status Solidi B* **140**, 407 (1987).
- ²³N. Shibata, A. Ohki, S. Zembutsu, and A. Katsui, *Jpn. J. Appl. Phys.* **27**, L487 (1988).
- ²⁴J. Gutowski, N. Presser, and G. Kudlek, *Phys. Status Solidi A* **120**, 11 (1990).
- ²⁵R. Baltrameyunas and E. Kuokshtis, *Fiz. Tverd. Tela (Leningrad)* **22**, 1009 (1980) [*Sov. Phys. Solid State* **22**, 589 (1980)].
- ²⁶J. Gutowski, I. Broser, and G. Kudlek, *Phys. Rev. B* **39**, 3670 (1989).